3 Solar (Light) Energy Harvesting

3.1 Introduction

The ubiquitous presence of sunlight makes solar energy one of the most abundant sources of ambient energy. Consequently, harvesting of light wave energy is one of the most important applications of energy harvesting technologies. This chapter presents the principles of solar cell operation and focuses on the challenges and optimization of light energy harvesting circuits and their integration with other harvester circuits and antennas, topics that are fundamental toward the implementation of energy autonomous wireless sensors.

The chapter begins with an introductory section describing the origins of solar cell technology. Next measures of light energy and the solar cell model and efficiency are presented. Finally, the integration of solar cells with antennas and the combination of various energy harvesting sources are discussed.

3.2 History

Solar energy harvesting, or more generally light energy harvesting, consists of converting energy contained in photons of light into electrical energy. This is a one-step process where a photon, a quantum of energy of light, is absorbed by an electron in a solid. The electron is excited in a higher energy state where it is able to move, generating an electric current [61].

This phenomenon was first studied by Edmond Bequerel in 1839 [62]. Bequerel observed that an electrical current was produced when two platine or gold electrodes dipped in a solution that can be acid, neutral, or alcaline are illuminated by unequal light intensity. This is known as the photovoltaic effect. Experiments by other researchers followed and, most notably, in 1876, William Adams and Richard Day observed an electrical current when a selenium sample in contact with two heated platinum contacts was illuminated by light [61]. The first solar cell is attributed to Charles Fritts, who installed the first rooftop solar panel by coating selenium with gold in 1894.

https://doi.org/10.1017/9781139600255.004 Published online by Cambridge University Press

When a semiconducting material such as silicon is illuminated by light, light photons with energy above the band gap of the material excite carriers, which results in an observed electrical current [6]. Specifically, electrons from the valence band of the semiconductor that absorb the incoming photons are excited into the conduction band, resulting in electron–hole pairs and therefore an increased conductivity. A piece of semiconducting material with ohmic contacts is a photoconductor. In order to be able to generate current and avoid the subsequent fast recombination of the electron–hole pairs, photodiodes are utilized instead of photoconductors [63]. There exist four types of photodiodes, namely p-i-n, p-n, heterojunction, and metal-semiconductor (Schottky barrier) photodiodes [64]. Conventional wafer type solar cells are p-n photodiodes, whereas thin-film solar cells are typically p-i-n photodiodes [63].

There are three generations of solar cells. The first generation includes wafer-based solar cells mainly built on silicon. The disadvantages of wafer-based solar cells are both high cost and low solar-to-electrical energy conversion efficiency. Approximately half of the cost of a Si wafer (c-Si) photovoltaic module is attributed to wafer preparation [63]. The second generation began in the early 1980s and includes thin film solar cells [65]. Thin film technology both reduced material costs and allowed a much larger size of the unit of manufacturing of approximately 100 times compared to the first-generation unit size, which was limited to the wafer size. In 2003, the production cost of first-generation technology was 150 USDm^{-2} with obtained efficiencies of 20%, whereas second-generation technology offered reduced production costs of 30 USDm^{-2} with lower efficiencies of 5%–10% [65].

Third-generation photovoltaic technology combines the low-cost fabrication of thin film technology with novel design concepts able to lead to much higher efficiencies. One such possibility is the use of tandem solar cells where two or more cells of different materials and band-gap energy are stacked on top of each other aiming to maximize the efficiency of photovoltaic conversion of photons with different energy [65]. Another approach is the possibility of exciting multiple electron–hole pairs from high-energy photons. Finally, another technique is the solar thermal electric one, where sunlight is first converted to heat and subsequently converted to electrical energy or reradiated as light (thermophotovoltaics).

Finally, an emerging solar cell technology is based on quantum dots. Quantum dots are semiconductor nanoparticles that have optoelectronic properties that are tunable according to their shape and size. Colloidal quantum dots are synthesized into thin films from liquid solutions, and they have shown a very promising potential in solar cell applications due to the ability to tune their band gap by modifying the fabrication conditions [66] and due to the possibility of large-scale fabrication using, for example, spin coating or inkjet printing methods [67]. They have been considered for single junction or tandem solar cell configurations exploring both the infrared and visible solar spectra [66].

https://doi.org/10.1017/9781139600255.004 Published online by Cambridge University Press

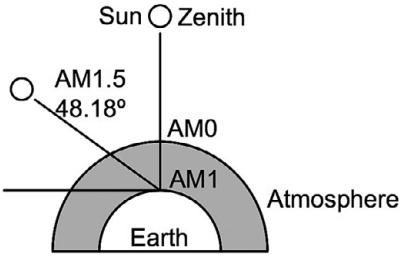

Figure 3.1 Air mass standards.

3.3 Light Sources and Measures

The various light sources are characterized by measuring their irradiance I_λ, which has units of power density (Wm^{-2}). Solar light with a power density of 1,000 Wm^{-2} (= 100 $mWcm^{-2}$) is also called 1 sun. The irradiance measures the power density of a radiated wave across the complete frequency spectrum. In contrast, the spectral irradiance consists of the irradiance per wavelength, and it is typically measured in $Wm^{-2}nm^{-1}$.

The irradiance should be distinguished from illuminance, which is a photometric measure with units lux or lumens per square meter (lux = lm m^{-2}), which measures the perceived power density of light weighted by the sensitivity of the human eye [68]. The sensitivity of the human eye is defined by a luminosity function. The visible light spectrum extends from 380 nm to 750 nm, while the solar spectral irradiance is typically provided in the 280 to 4,000 nm interval.

The American Society for Testing and Materials (ASTM) has developed the standard solar spectral irradiance distributions that are used in evaluating solar cell performance [69]. The air mass zero (AM0) or extraterrestrial (ETR) irradiance spectrum is provided in the standard ASTM E-490-00 developed in 2000 [70] based on several sets of measured data from satellites or space missions. The total solar irradiance of AM0 is 1.366 KWm^{-2}, known as the solar constant [69]. Additionally, ASTM defines two terrestrial solar irradiance distributions, the AM1.5 Global (AM1.5G) and the AM1.5 Direct and Circumsolar (AM1.5D), included in the standard ASTM-G-173-03 [70]. Both distributions are defined assuming a surface that is receiving the solar radiation that has a tilt of 37° toward the Earth's equator. The tilt angle selected is approximately the average latitude for the contiguous U.S.A. The air mass AM quantity is derived from the length of the path that the solar radiation waves are passing through within the earths atmosphere. An air mass of 1 (AM1) corresponds to a solar zenith angle of 0°. The AM1.5 standard distributions correspond to a solar zenith angle of 48.18° as shown in Figure 3.1.

The global spectral irradiance distribution includes both direct and diffuse solar radiation and has a total irradiance of 1 sun = 1 KWm^{-2}. The direct and circumsolar distribution does not include diffuse radiation, and it corresponds to

https://doi.org/10.1017/9781139600255.004 Published online by Cambridge University Press

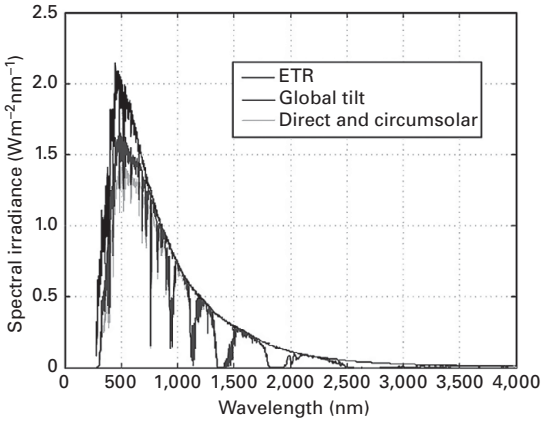

Figure 3.2 Standard solar spectral irradiance distributions.

an irradiance of 0.9 KWm^{-2} [7]. The three standard distributions are shown in Figure 3.2.

Indoor light sources have a much lower irradiance between 100 and 1,000 times less than outdoor sunlight. Specifications for indoor light sources are usually given in photometric units, with a typical minimum value of 500 lux required for libraries and offices [8]. The AM1.5 global spectrum corresponds to 100 Klux in photometric units. However, the actual levels of solar irradiance can vary significantly from the values specified in the AM1.5 standards due to many factors such as the daily variation of the air mass that solar radiation has to travel through during a single day as the position of the sun varies relative to the earth, and due to the presence of clouds that scatter direct sunlight. It is reported in [71] that the average solar irradiance on earth is 170 Wm^{-2} which is approximately one sixth of the AM1.5G standard irradiance.

3.4 Efficiency of Solar Cells

The most important parameter in characterizing the performance of solar cells is their efficiency. The efficiency η is defined as the ratio of the electrical power generated by the solar cell P_o to the incident light power P_i.

$$\eta = P_o/P_i \tag{3.1}$$

The incident power is the integral of the irradiance I_λ over the surface A of the solar cell, which for a uniform irradiance is given by

$$P_i = I_\lambda A. \tag{3.2}$$

The theoretical calculation of the output power of the solar cell requires the application of solid-state theory and thermodynamics. There are several

https://doi.org/10.1017/9781139600255.004 Published online by Cambridge University Press

theoretical works dealing with the efficiency of solar cells; however, a widely used model was proposed by Shockley and Queisser [72].

In computing the efficiency of solar cells, Shockley and Queisser assumed that the source of light energy, the sun, and the solar cell itself behave as black bodies with temperature T_s and T_c respectively. In [72], it was postulated that the solar cell efficiency depends on four parameters, namely the energy band gap E_g of the material comprising the solar cell, the ratio between the temperature of the sun T_s and the temperature of the solar cell T_c, the probability t that a photon with energy above the band gap will excite an electron to the conduction band and generate an electron–hole pair and a geometric factor f_w related to the angle subtended by the sun toward the solar cell. This is expressed as

$$\eta = \eta(x_g, x_c, t, f_w), \tag{3.3}$$

where

$$x_g = E_g/kT_s \tag{3.4}$$

$$x_c = T_c/T_s \tag{3.5}$$

and $k = 1.38064852 \cdot 10^{-23}$ m^2 kg s^{-2} K^{-1} is Boltzmann's constant. In (3.3) the normalized energy parameters x_g and x_c were used, similarly to [72]. Shockley and Queisser computed the ultimate efficiency limit and the detailed balanced efficiency limit for p-n junction solar cells, which will be described next. In the following, the probability t is assumed to be equal to one.

3.5 Ultimate Solar Cell Efficiency

The ultimate solar cell efficiency η_g depends only on the energy band gap E_g of the material comprising the solar cell and the temperature of the sun T_s expressed through the single parameter x_g [72].

Every photon with energy $E = h \cdot f > h \cdot f_g = E_g$, where f is the frequency of the photon and $h = 6.62607004 \cdot 10^{-34}$ m^{2}kg s^{-1} is Planck's constant, excites a single electron to the conduction band. Because the sun is considered a black body with temperature T_s it radiates photons whose energy follows the Planck distribution.

The number of photons Q with energy between two limits E_1 and E_2 for a black body described by a Plank distribution with temperature T, is calculated by integrating the Planck distribution from E_1 to E_2,

$$Q(T, E_1, E_2) = \frac{2\pi}{h^3 c^2} \int_{E_1}^{E_2} \frac{E^2 dE}{e^{E/kT} - 1} \tag{3.6}$$

Therefore, the number of photons Q_s with energy larger than E_g takes the form $Q_s = Q(T_s, E_g, +\infty)$, which is computed as

https://doi.org/10.1017/9781139600255.004 Published online by Cambridge University Press

$$Q_s = Q(T_s, E_g, +\infty) = \frac{2\pi}{c^2}\int_{f_g}^{\infty} \frac{f^2 df}{e^{hf/kT_s} - 1} = \frac{2\pi (kT_s)^3}{h^3 c^2}\int_{x_g}^{\infty} \frac{x^2 dx}{e^x - 1}. \quad (3.7)$$

It is further assumed that the excited electrons quickly lose any excess energy above E_g as thermal energy. The total output power available by the solar cell is then

$$P_o = h f_g Q_s A. \quad (3.8)$$

The irradiance I_λ of the light impinging the solar cell is given by integrating the Planck distribution from 0 to $+\infty$,

$$I_\lambda = \frac{2\pi h}{c^2}\int_0^{\infty} \frac{f^3 df}{e^{hf/kT_s} - 1} = \frac{2\pi (kT_s)^4}{h^3 c^2}\int_0^{\infty} \frac{x^2 dx}{e^{hx} - 1} = \frac{2\pi^5 (kT_s)^4}{15 h^3 c^2} = \sigma T_s^4, \quad (3.9)$$

where $\sigma = 5.670367 \text{J m}^{-2}\text{s}^{-1}\text{K}^{-4}$ is the Stefan–Boltzmann constant. Using (3.2), (3.8), (3.7), and (3.9), one gets

$$\eta_g = \frac{E_g Q_s}{I_\lambda} = \frac{h f_g Q_s}{I_\lambda} = \frac{15 x_g}{\pi^4}\int_{x_g}^{\infty} \frac{x^2 dx}{e^x - 1}. \quad (3.10)$$

One can easily compute numerically (3.10) for different energy band-gap values and a given sun temperature. Shockley and Queisser showed that the ultimate efficiency η_g has a maximun value of 44% corrseponding to a normalized band gap of $x_g = 2.2$ (or $E_g = 1.1$ eV) assuming a sun temperature of 6,000 K. The energy unit electon-volt 1 eV $= 1.60217662 \cdot 10^{-19}$ J is typically used in solid-state physics. A more accurate ultimate efficiency value can be computed by considering a sun temperature of 5,800 K or by integrating a measured solar spectrum such as the AM0 or AM1.5 instead of the Planck distribution [73].

3.6 Detailed Balance Limit

In order to compute a more accurate efficiency value, Schockley and Queisser [72] considered the various contributions to the generation and recombination of carriers in the solar cell, thus defining the detailed balance limit of the solar cell efficiency. There are five different contributions to the carrier generation and recombination, namely, (a) the generation of electron–hole pairs due to the absorption of the incident solar radiation with rate F_s; (b) radiative recombination of electron–hole pairs with rate $F_c(V)$; (c) removal of electron–hole pairs due to current generation from the solar cell with rate I/q and finally other nonradiative processes that result in (d) generation with rate $R(0)$; and (e) recombination with rate $R(V)$ of electron–hole pairs. The voltage V is the voltage between the p and n regions of the solar cell. In the steady-state condition, all the preceding processes are balanced, resulting in

$$I/q = F_s - F_c(V) + R(0) - R(V) \quad (3.11)$$

https://doi.org/10.1017/9781139600255.004 Published online by Cambridge University Press

$$I = q\left[F_s - F_{c0}\right] + q\left[F_{c0} - F_c(V) + R(0) - R(V)\right], \tag{3.12}$$

where $F_{c0} = F_c(0)$. In the next paragraphs, we will consider the different processes separately in order to express the steady-state equation in a more practical form

$$\begin{aligned} I &= I_s + I_d = I_s - I_0\left[e^{(V/V_c)} - 1\right] \\ I_s &= q\left[F_s - F_{c0}\right] \\ I_d &= -q\left[F_{c0} - F_c(V) + R(0) - R(V)\right], \end{aligned} \tag{3.13}$$

where the different current components are identified as the short-circuit current I_s and the dark current I_d, with $I_0 = q\left[F_{c0} + R(0)\right]$, $V_c = kT_c/q$.

3.6.1 Generation of Electron–Hole Pairs Due to Solar Radiation

In order to compute the generation rate of hole–electron pairs, one first needs to compute the incident solar radiation. In computing the ultimate solar cell efficiency, it was assumed that all the power emitted from the sun reaches the solar cell, which was considered a black body with temperature T_s (3.9). A black body, however, radiates isotropically, and therefore only a fraction of the radiated power reaches the solar cell. In fact, the total number of photons per unit time reaching the surface of the solar cell is equal to the rate of generation of electron–hole pairs

$$F_s = f_w A Q_s, \tag{3.14}$$

where we assumed as before that the probability of excitation of a hole–electron pair by a photon with energy above the band gap E_g is one. A geometrical factor f_w has been introduced that depends on the solid angle ω_s subtended by the sun and the angle of incidence upon the solar cell.

The solid angle subtended by the sun is

$$\omega_s = \pi(D/L)^2/4 = 6.85 \cdot 10^{-5}\text{sr}, \tag{3.15}$$

where $D = 1.39 \cdot 10^6$ km is the diameter of the sun and $L = 149 \cdot 10^6$ km the distance of the sun to the earth and the solar cell.

Assuming a planar flat solar cell, the angle of incidence of the solar radiation is defined as the angle θ between the normal to the solar cell and the direction of the sun. In this case, the geometrical factor f_w becomes [72]

$$f_w = \omega_s \cdot \cos(\theta)/\pi. \tag{3.16}$$

In the case of normal incidence, the geometrical factor becomes $f_w = \omega/\pi = 2.18 \cdot 10^{-5}$.

Finally, the total incident power to the solar cell becomes

$$P_{in} = f_w A I_\lambda = f_w A \sigma T_s^4. \tag{3.17}$$

https://doi.org/10.1017/9781139600255.004 Published online by Cambridge University Press

3.6.2 Radiative Recombination of Electron–Hole Pairs

In order to compute the recombination rate F_c of electron–hole pairs, Schockley and Queisser assumed that the solar cell is surrounded by a black body of temperature T_c. The recombination rate is proportional to the the number of electrons per unit area n in the conduction band and the number of holes per unit area p in the valence band, i.e., $F_c \propto np$.

In the equilibrium state, where no external perturbations such as the absorption of photons from the sun affect the solar cell, the rate of photons impinging to the solar cell by the surrounding black body is equal to the rate of photons radiated by the solar cell due to the recombination of electron–hole pairs. Consequently, no net current generation is observed. Similarly to the previous section, the rate of incident photons with energy above the bandgap is equal to

$$F_{c0} = 2AQ_c, \tag{3.18}$$

where $Q_c = Q(T_c, E_g, +\infty)$ the number of photons per unit time and area with energy above E_g computed by appropriately integrating Planck's distribution with temperature T_c. It is also assumed that each photon with such energy has a probability equal to 1 to generate an electron–hole pair. Furthermore, since the black body surrounds the solar cell, the total area of the cell is equal to $2A$ and the geometrical factor f_w is equal to one.

In the equilibrium state, the number of electrons per unit area n in the conduction band and the number of holes per unit area p in the valence band of the semiconductor are related by [61, 64]

$$np = n_i^2, \tag{3.19}$$

where $n_i \propto e^{-E_g/kT}$ is the intrinsic carrier density that depends on the bandgap energy E_g. When the solar cell is illuminated by an external light source such as the sun and electron–hole pairs are generated due to the absorption of photons, the solar cell is not in equilibrium and the carrier densities do not obey (3.19). However, when the disturbance is not very large and not too fast changing, the carrier densities reach a quasithermal equilibrium state that is modeled as a small perturbation of the original thermal equilibrium state [61, 64]. The carrier generation results in a chemical potential qV difference between the Fermi levels corresponding to the electrons and holes, where V is equal to the voltage generation across the semiconductor solar cell terminals. The electron and hole density product is then given

$$np = n_i^2 e^{V/V_c}. \tag{3.20}$$

Consequently, in the nonequilibrium case, the rate of radiative recombination becomes [72]

$$F_c(V) = F_{c0} e^{V/V_c}. \tag{3.21}$$

https://doi.org/10.1017/9781139600255.004 Published online by Cambridge University Press

3.6.3 Nonradiative Generation and Recombination of Electron–Hole Pairs

The nonradiative generation and recombination rates of electron–hole pairs are defined as $R(0)$ and $R(V)$ respectively. Similarly to their radiative counterparts, they are also equal when the solar cell is in the equilibrium state, and they depend on the chemical potential qV in the nonequilibrium state as

$$R(V) = R(0)e^{V/V_c}. \tag{3.22}$$

Shockley and Queisser further assumed that the nonradiative processes are only a fraction of the radiative ones defined by the ratio $f_c = F_{c0}/(F_{c0} + R(0)$. Using 3.21 and 3.22, one obtains an expression for the dark current

$$\begin{aligned} I_d &= -q\left[F_{c0} - F_c(V) + R(0) - R(V)\right] \\ &= q\left[F_{c0} + R(0)\right]\left[e^{(V/V_c)} - 1\right] \\ &= I_0\left[e^{(V/V_c)} - 1\right], \end{aligned} \tag{3.23}$$

where

$$I_0 = q\left[F_{c0} + R(0)\right] = \frac{qF_{c0}}{f_c} = \frac{2qAQ_c}{f_c}. \tag{3.24}$$

3.6.4 The Short-Circuit Current and the Open-Circuit Voltage

The short-circuit current I_s and the open-circuit voltage V_{oc} are two important parameters characterizing the performance of a solar cell. The results of the previous section provide some insight into these two important parameters. One can find a relation between the two by setting $I = 0$ and $V = V_{oc}$ in (3.13) and solving for V_{oc} or I_s

$$\begin{aligned} V_{oc} &= V_c \ln\left(1 + \frac{I_s}{I_o}\right) \\ I_s &= I_o\left(e^{\frac{V_{oc}}{V_c}} - 1\right). \end{aligned} \tag{3.25}$$

The short-circuit current was defined from (3.12) and (3.13) to be

$$I_s = q\left[F_s - F_{c0}\right]. \tag{3.26}$$

We proceed by normalizing the expression of I_s using the saturation current I_o (3.24) to write

$$\frac{I_s}{I_o} = f_c\left[\frac{F_s}{F_{c0}} - 1\right]. \tag{3.27}$$

Finally, using (3.14) and (3.21), one obtains

$$\frac{I_s}{I_o} = f_c\left[\frac{f_w}{2}\frac{Q_s}{Q_c} - 1\right] \approx \frac{f_c f_w}{2}\frac{Q_s}{Q_c}. \tag{3.28}$$

https://doi.org/10.1017/9781139600255.004 Published online by Cambridge University Press

The number of photons $Q(T, E_g, +\infty)$ with energy at least E_g emitted from a black body at temperature T_s has an exponential dependence on the band-gap energy E_g [72]

$$Q(T, E_g, +\infty) \approx A(T) e^{\frac{-E_g}{kT}}, \tag{3.29}$$

where $A(T)$ is a constant that depends on the temperature T. Using 3.29, one can obtain the dependence of the short-circuit current on the band-gap energy E_g

$$\frac{I_s}{I_o} \approx \frac{f_c f_w}{2} \frac{A(T_s)}{A(T_c)} e^{E_g/kT_c}. \tag{3.30}$$

Finally, using (3.25) and (3.30) one obtains the dependence of the open-circuit voltage on the band-gap energy

$$\begin{aligned} \frac{V_{oc}}{V_c} &= \ln\left[(1 - f_c) + \frac{f_c f_w}{2} \frac{Q_s}{Q_c}\right] \approx \ln\left[\frac{f_c f_w}{2} \frac{Q_s}{Q_c}\right] \\ \frac{V_{oc}}{V_c} &\approx \frac{E_g}{kT_c} + \ln\left[C(f_c, f_w, T_s, T_c)\right]. \end{aligned} \tag{3.31}$$

The constant C is smaller than 1, and consequently the open-circuit voltage is always smaller than the band-gap voltage E_g/q and becomes equal to it as temperature T_c tends to 0 K [72].

3.7 Circuit Model of Solar Cells

The current voltage characteristic of the solar cell is given by (3.13), which is repeated here for convenience.

$$I = I_s + I_d = I_s - I_0\left[e^{(V/V_c)} - 1\right]. \tag{3.32}$$

This is expressed in a circuit schematic as a current source in parallel with an ideal diode shown in Figure 3.3. When the equilibrium of the solar cell is perturbed by an external source of photons, additional carriers are generated in the cell. If the solar cell is connected to a load, then a current is generated. The value of this current corresponds to the short-circuit current I_s, and it is equal to the current due to the additional carriers qF_s minus a quantity qF_{c0} due to the recombination of carriers at thermal equilibrium [72], given in (3.13). Furthermore, as the external perturbation results in a quasithermal equilibrium, a voltage V is developed across the cell, which results in a current with opposite polarity called the dark current I_d of the solar cell. The dark current is equal to the current that flows across the solar cell if there is an external voltage V applied to its terminals in the dark (i.e., without any external light source applied). As one can immediately identify, the dark current expression is similar to that of an ideal diode.

The nonideal solar cell model also includes parasitic series R_s and parallel R_p resistances that represent thermal losses included in Figure 3.3. The series

https://doi.org/10.1017/9781139600255.004 Published online by Cambridge University Press

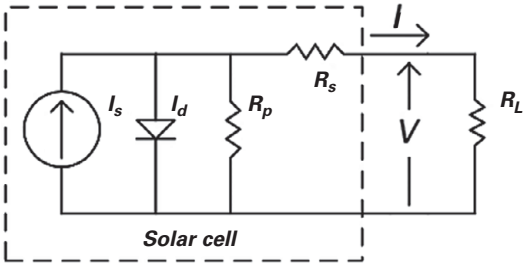

Figure 3.3 Circuit model of the solar cell.

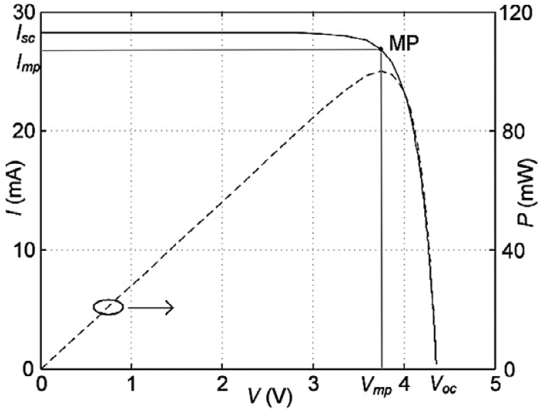

Figure 3.4 Current to voltage characteristic of an ideal solar cell.

resistance is typically due to the terminal contacts of the cell and the parallel resistance due to leakage current around the sides of the device [61]. The current voltage characteristic of a nonideal solar cell becomes

$$I = I_s - I_0 \left[e^{\frac{V+IR_s}{V_c}} - 1 \right] - \frac{V + IR_s}{R_p}. \tag{3.33}$$

3.8 The Detailed Balance Limit of Maximum Efficiency

The solar cell current to voltage I-V characteristic has the shape shown in Figure 3.4. Being a current source, the solar cell generates an approximately constant current for a wide range of voltage values across its terminals, which corresponds to different output loads connected to the solar cell. On one hand, as the load resistance becomes very small the solar cell current tends to its limiting value corresponding to the short-circuit current value I_s. On the other hand, as the load resistance takes large values the solar cell characteristic approaches the open-circuit voltage V_{oc}. The slope of the I-V characteristic near the I_s and

https://doi.org/10.1017/9781139600255.004 Published online by Cambridge University Press

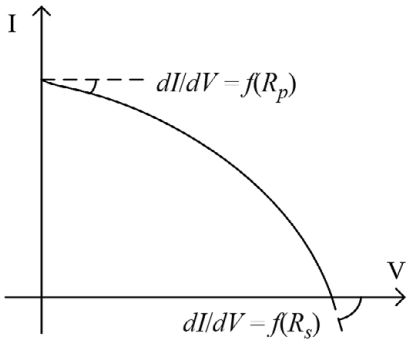

Figure 3.5 Effect of parasitic resistances on the current to voltage characteristic of a solar cell.

V_{oc} limiting values is dependent on the parasitic resistance R_s and R_p values respectively, as shown in Figure 3.5.

Due to the nonlinear nature of the I-V characteristic, there exists an optimum load value for a given solar irradiance or I_s, for which a maximum power P_m is delivered to the load as Figure 3.4 shows. This value, in effect, corresponds to the detailed balance limit of efficiency. The optimum voltage V_m can be obtained by taking the derivative of power versus the voltage and setting it equal to zero $dP/dV = d(IV)dV = 0$, which gives

$$\left(1 + \frac{V_m}{V_c}\right) e^{\frac{V_m}{V_c}} = e^{\frac{V_{oc}}{V_c}} = 1 + \frac{I_s}{I_o}. \tag{3.34}$$

The optimum voltage can be obtained by multiplying (3.34) with e in order to bring the left side to the form xe^x and using the definition of the Lambert function W to obtain

$$\frac{V_m}{V_c} = W_o\left(e(1 + I_s/I_o)\right) - 1 = W_o\left(e^{(1+V_{oc}/V_c)}\right) - 1, \tag{3.35}$$

where the principal branch W_o of the Lambert function is used because its argument takes positive values. The optimum current value I_m is then found solving (3.34) for e^{V_m/V_c} and substituting the obtained value in (3.13).

$$\frac{I_m}{I_o} = (1 + I_s/I_o)\left(\frac{V_m/V_c}{1 + V_m/V_c}\right) \tag{3.36}$$

Using (3.35) and (3.36), one can obtain an expression for the maximum output power from the solar cell $P_m = I_m V_m$,

$$P_m = (I_s + I_o)\frac{V_c\left(W_o\left(e(1 + I_s/I_o)\right) - 1\right)^2}{W_o\left(e(1 + I_s/I_o)\right)}. \tag{3.37}$$

The maximum power P_m is graphically given by a rectangle with sides equal to I_m and V_m. The values I_m and V_m are a fraction of I_s and V_{oc} respectively, which depends on (3.13) and (3.35). The fill factor FF expresses how close the product $I_m V_m$ is to the product $I_s V_{oc}$

https://doi.org/10.1017/9781139600255.004 Published online by Cambridge University Press

$$FF = \frac{I_m V_m}{I_s V_{oc}}, \tag{3.38}$$

which represents a maximum possible power value for a given solar irradiance and solar cell and provides a measure of the quality of the solar cell. The detailed balance limit of efficiency is given

$$\eta = \frac{I_m V_m}{P_{in}} = \frac{FF I_s V_{oc}}{P_{in}}, \tag{3.39}$$

where the input power $P_{in} = f_w A I_\lambda = f_w A \sigma T_s^4$ has been derived in (3.17). Using (3.13), (3.14), (3.17), (3.21), (3.24), and (3.37), one obtains an expression for the maximum efficiency limit, which depends on T_s, T_c, f_w, f_c, and E_g,

$$\eta = \left[\frac{qQ_s}{I_\lambda}\right]\left[1 + \frac{2(1-f_c)}{f_c f_w}\frac{Q_c}{Q_s}\right]\frac{V_c\left[W_o\left(e(\frac{f_c f_w}{2}\frac{Q_s}{Q_c} + (1-f_c))\right) - 1\right]^2}{W_o\left(e(\frac{f_c f_w}{2}\frac{Q_s}{Q_c} + (1-f_c))\right)} \tag{3.40}$$

or, using the expression for the ultimate efficiency η_g (3.10),

$$\eta = \eta_g \eta_{sr} \tag{3.41}$$

with

$$\eta_{sr} = \left[\frac{qV_c}{E_g}\right]\left[1 + \frac{2(1-f_c)}{f_c f_w}\frac{Q_c}{Q_s}\right]\frac{\left[W_o\left(e(\frac{f_c f_w}{2}\frac{Q_s}{Q_c} + (1-f_c))\right) - 1\right]^2}{W_o\left(e(\frac{f_c f_w}{2}\frac{Q_s}{Q_c} + (1-f_c))\right)}, \tag{3.42}$$

where the effect of the geometrical considerations and of the radiative recombination in reducing the ultimate efficiency η_g has been included in the term η_{sr}. If one does not consider any nonradiative recombination processes $f_c = 1$, then the expression for the efficiency is simplified to

$$\eta = \eta_g \eta_{sr} = \eta_g \frac{qV_c}{E_g}\frac{\left[W_o\left(e(\frac{f_w}{2}\frac{Q_s}{Q_c})\right) - 1\right]^2}{W_o\left(e(\frac{f_w}{2}\frac{Q_s}{Q_c})\right)}. \tag{3.43}$$

Using the preceding theory, Schockley and Queisser [72] calculated the detailed balance limit of efficiency of solar cells for different parameter values, by deriving numerically the maximum current and voltage using the condition (3.34). The formulation obtained previously using the Lambert function provides an intuitive expression for the efficiency giving the same numerical result.

The efficiency for $T_s = 6{,}000$ K, $T_c = 300$ K, $f_w = 2.18 \cdot 10^{-5}$ and no nonradiative recombination $f_c = 1$ is plot in Figure 3.6. The numerical results showed that the maximum efficiency is approximately 30.5% for a band-gap energy $E_g = 1.314$ eV, whereas the maximum efficiency for Silicon with band-gap energy $E_g = 1.1$ eV is approximately 29.5% [72]. A more accurate efficiency limit can be obtained by considering a measured solar spectrum such as the AM0 or the AM1.5 instead of the Planck distribution [73].

https://doi.org/10.1017/9781139600255.004 Published online by Cambridge University Press

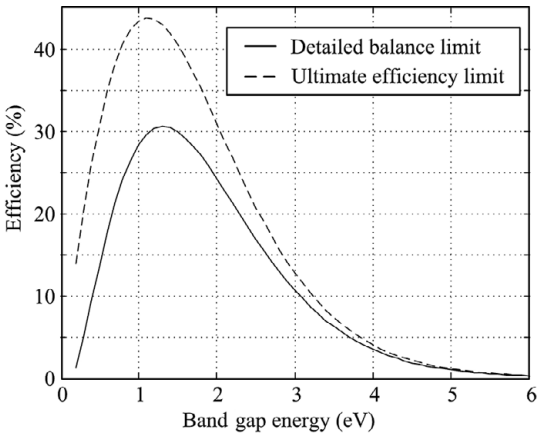

Figure 3.6 Ultimate efficiency and detailed balance efficiency limit versus bandgap energy E_g ($T_s = 6{,}000$ K, $T_c = 300$ K, $f_w = 2.18 \cdot 10^{-5}$ and no nonradiative recombination $f_c = 1$).

The four quantities I_s, V_{oc}, FF, and η are commonly used to compare the performance of different solar cells under various standard conditions such as $T_c = 25°$ C and AM1.5G solar irradiance. Comparison tables are published periodically in the literature [74]. Table 3.1 illustrates measured values of these parameters for a selective set of different solar cell technologies based on the data published in [74]. One can see that silicon solar cell performance is approaching the detailed balance efficiency limit, while the best efficiency to date is obtained by GaAs solar cells.

Table 3.1 Selected maximum measured solar cell performance parameters under AM1.5G solar irradiance at $T = 25\ ^\circ$ C [74].

Technology	Efficiency (%)	V_{oc} (V)	I_s/A (mAcm^{-2})	FF (%)
Crystalline Si	26.7	0.738	42.65	84.9
Multicrystalline Si	22.3	0.6742	41.08	80.5
Amorphous Si	10.2	0.896	16.36	69.8
Thin film GaAs	29.1	1.1272	29.78	86.7
CIGS	22.9	0.744	38.77	79.5
CdTe	21.0	0.8759	30.25	79.4
Perovskite	20.9	1.125	24.92	74.5
Dye sensitized	11.9	0.744	22.47	71.2
Organic	11.2	0.78	19.30	74.2

https://doi.org/10.1017/9781139600255.004 Published online by Cambridge University Press

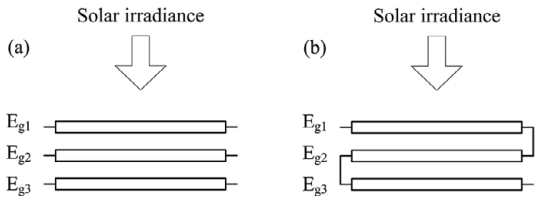

Figure 3.7 Architecture of a tandem solar cell: (a) unconstrained and (b) series connected.

3.9 Efficiency Limits for Tandem Solar Cells

It is possible to increase the overall efficiency of a solar cell by forming a stack of solar cells where each cell has an energy band gap that is optimum for converting to electrical energy the energy of the photons of a specific energy range (or equivalently frequency range) within the solar spectrum. These are called tandem solar cells [65].

We assume that a solar cell absorbs all photons with energy above its band gap and it is transparent to all photons with energy less than its band gap. This way we visualize a tandem cell comprising a stack of individual cells. Each solar cell in the tandem absorbs photons both from the solar radiation that reaches its surface and from the remaining solar cells of the tandem [75]. Due to the difference in temperatures between the sun and the solar cells, the amount of radiation from the remaining solar cells can be ignored when the number of cells in the tandem is small [75]. The top cell of the tandem, which the solar radiation reaches first, has the highest band-gap energy (E_{g1}), and the bad-gap energy of the subsequent cells in the stack is progressively reduced ($E_{g1} > E_{g2} > E_{g3} > \ldots$). The first (top) solar cell absorbs all photons with energy $E > E_{g1}$, the second cell absorbs photons with energy $E_{g2} < E < E_{g1}$, the third $E_{g3} < E < E_{g2}$, and so on. We may assume that the outputs of each solar cell are independent, resulting in what is called an unconstrained cell, or that they are connected in series [76]. The structure of the tandem cell is conceptually shown in Figure 3.7. The series connection imposes an additional constraint in the tandem cell in that the current through all solar cells has to be equal.

Therefore, both in the unconstraint and in the series connected tandem cell the band-gap energies of the individual cells may be optimized in order to find the values that lead to a maximum obtained efficiency. In order to compute the optimum band-gap energies, it is possible to consider either the ultimate solar cell efficiency (Section 3.5) or the detailed balance limit of efficiency (Section 3.8) and model the solar radiation either as a blackbody or using measured spectra such as the AM1.5G spectrum.

Based on the preceding, in order to compute the solar cell efficiency of the tandem cell we will need to integrate the Plank distribution corresponding to a blackbody with temperature T between two energy limits E_1 and E_2, defined

https://doi.org/10.1017/9781139600255.004 Published online by Cambridge University Press

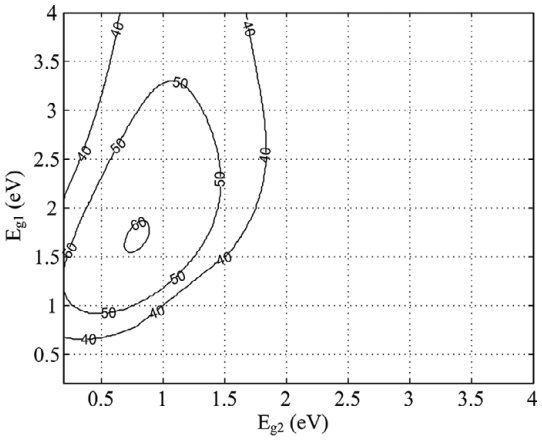

Figure 3.8 Ultimate efficiency limit for a tandem solar module comprising two cells with different band-gap energy.

in Equation (3.6). Using the efficiency formulations derived in Sections (3.5) and (3.8), we have computed efficiency contours for a two band-gap tandem cell modeling the solar radiation as a blackbody with $T_s = 6{,}000$ K. The ultimate efficiency for each solar cell is computed based on Equation (3.10), where the integral of the Planck distribution Q is computed using the appropriate energy limits for each solar cell in the tandem. The ultimate efficiency of the tandem cell becomes

$$\eta_g = \frac{E_{g1}Q_{s1} + E_{g2}Q_{s2}}{I_\lambda} \tag{3.44}$$

with $Q_{s1} = Q(T_s, E_{g1}, +\infty)$ and $Q_{s2} = Q(T_s, E_{g2}, E_{g1})$. The results corresponding to the ultimate efficiency limit for an unconstrained tandem are shown in Figure 3.8. The optimum band-gap energies corresponding are found to be approximately 0.78 eV and 1.7 eV.

The detailed efficiency limit was also computed in Figure 3.9 assuming $T_c = 300$ K, $f_w = 2.18 \cdot 10^{-5}$ and no radiative recombination. In this case, the efficiency is found based on (3.40) with $f_c = 1$. The detailed efficiency limit of the tandem cell takes the form

$$\eta = \frac{I_{m1}V_{m1} + I_{m2}V_{m2}}{P_{in}}, \tag{3.45}$$

where $P_{m1} = I_{m1}V_{m1}$ and $P_{m2} = I_{m2}V_{m2}$ are the maximum power values from each cell in the tandem and the input power $P_{in} = f_w A I_\lambda = f_w A \sigma T_s^4$ has been defined in (3.17). The maximum voltage and current of a solar cell have been defined in (3.35) and (3.36) respectively and for $f_c = 1$ using (3.28) and (3.24), they become

$$V_m = V_c \left[W_o \left(e \left(\frac{f_w Q_s}{2Q_c} \right) \right) - 1 \right] \tag{3.46}$$

https://doi.org/10.1017/9781139600255.004 Published online by Cambridge University Press

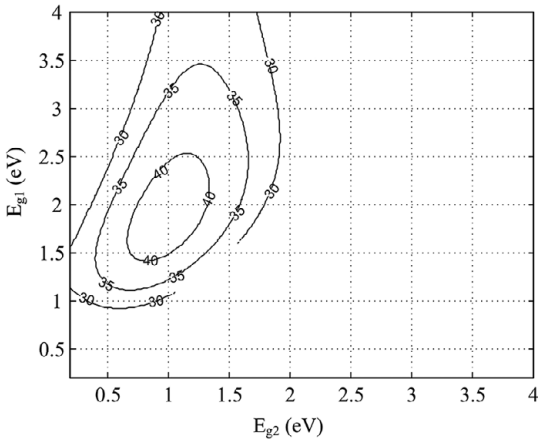

Figure 3.9 Detailed balance efficiency limit for a tandem solar module comprising two cells with different band-gap energy.

$$I_m = qAf_wQ_s\frac{\left[W_o\left(e\left(\frac{f_wQ_s}{2Q_c}\right)\right)-1\right]}{W_o\left(e\left(\frac{f_wQ_s}{2Q_c}\right)\right)}. \tag{3.47}$$

For the two solar cells of the tandem, the various integrals of the Planck distribution become $Q_{c1} = Q(T_c, E_{g1}, +\infty)$, $Q_{c2} = Q(T_c, E_{g2}, +\infty)$ and, as before, $Q_{s1} = Q(T_s, E_{g1}, +\infty)$, $Q_{s2} = Q(T_s, E_{g2}, E_{g1})$. This way, the detailed efficiency limit of the tandem solar cell becomes

$$\eta = \frac{qV_c}{I_\lambda}\left[\frac{Q_{s1}\left[W_o\left(e(\frac{f_w}{2}\frac{Q_{s1}}{Q_c1})\right)-1\right]^2}{W_o\left(e(\frac{f_w}{2}\frac{Q_{s1}}{Q_c1})\right)}+\frac{Q_{s2}\left[W_o\left(e(\frac{f_w}{2}\frac{Q_{s2}}{Q_c2})\right)-1\right]^2}{W_o\left(e(\frac{f_w}{2}\frac{Q_{s1}}{Q_c2})\right)}\right]. \tag{3.48}$$

Finally, Figure 3.10 shows the computed detailed efficiency limit in the case of a series constrained tandem cell. In this case, we must limit the maximum current of the tandem cell to the value corresponding to the smaller of the two cells and then compute the corresponding maximum voltage values. This is done, for example, defining an intermediate parameter X as follows:

$$X = \min\left\{Q_{s1}\frac{\left[W_o\left(e\left(\frac{f_wQ_{s1}}{2Q_{c1}}\right)\right)-1\right]}{W_o\left(e\left(\frac{f_wQ_{s1}}{2Q_{c1}}\right)\right)}, Q_{s2}\frac{\left[W_o\left(e\left(\frac{f_wQ_{s2}}{2Q_{c2}}\right)\right)-1\right]}{W_o\left(e\left(\frac{f_wQ_{s2}}{2Q_{c2}}\right)\right)}\right\}. \tag{3.49}$$

The series current is then defined with the help of X as follows:

$$I_m = qAf_wX. \tag{3.50}$$

Having found the current through the solar cell I_m, we can solve (3.13) to compute the solar cell voltage,

$$V_m = V_c\ln\left[1+\frac{I_s-I_m}{I_o}\right], \tag{3.51}$$

https://doi.org/10.1017/9781139600255.004 Published online by Cambridge University Press

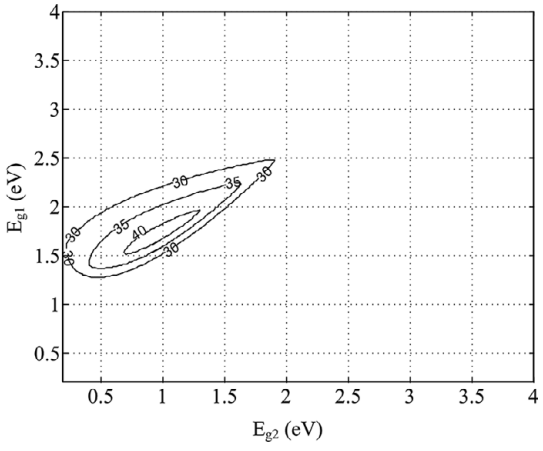

Figure 3.10 Detailed balance efficiency limit for a tandem solar module comprising two series connected cells with different band-gap energy.

where $I_o = 2qAQ_c$ is found from in (3.24) using $f_c = 1$. Additionally using (3.28), this becomes for each of the two solar cell voltages

$$V_{m1} = V_c \ln\left[\frac{f_w}{2} \cdot \frac{Q_{s1} - X}{Q_{c1}}\right] \tag{3.52}$$

and

$$V_{m2} = V_c \ln\left[\frac{f_w}{2} \cdot \frac{Q_{s2} - X}{Q_{c2}}\right]. \tag{3.53}$$

Finally, the detailed efficiency of the tandem cell becomes

$$\eta = \frac{I_m(V_{m1} + V_{m2})}{f_w A I_\lambda} = \frac{qX(V_{m1} + V_{m2})}{I_\lambda}. \tag{3.54}$$

The maximum efficiency of the unconstrained tandem cell with two cells was found to be 42.3% and for the series connected tandem 41.7%. This value represents a substantial increase compared to the maximum efficiency of a single cell of 30.5% shown in Figure 3.6. This formulation can easily be extended to a tandem cell with more than two cells.

3.10 Solar Antennas and Rectennas

Solar antennas integrate solar panels with antennas and have been originally proposed for satellite applications [77]. As a result, antenna and solar panel arrays have been developed [78, 79]. The immediate advantage of integrating solar cells and antennas is that of reducing size and consequently cost. The recent interest in extending the energy autonomy of wireless sensor nodes in the context of the Internet of Things (IoT) has resulted in design efforts focusing on low-profile

https://doi.org/10.1017/9781139600255.004 Published online by Cambridge University Press

solar antennas implemented in rigid substrates [80], transparent substrates [81], and also flexible substrates including paper, plastic polyethylene terephthalate (PET) [82], and textiles [83].

In the design of solar antennas, different types of printed antennas can be used, including patch or dipole/monopole antennas on the one hand and slot type antennas [79] on the other hand. Furthermore, the design process takes advantage of the fact that solar cells typically include a conductive (mirror) layer that can be integrated on top of the conductive surface of the antenna, or alternatively play the role of the conductive surface of the antenna itself if the layer conductivity is sufficiently high [79]. The design process consists of identifying through electromagnetic simulation the optimal placement of the solar cell in order not to disturb the radiation and impedance properties of the antenna. Another design challenge is that of identifying the proper placement of the wiring associated with the terminals of the solar cell and embedding it in the radiating structure. In this case, it is often common to connect one of the solar cell terminals (e.g., the dc ground) directly onto one of the conducting surfaces of the antenna, while the second terminal must be carefully wired in order not to disturb the radiating fields of the antenna.

An example of an ultrawideband monopole on PET substrate with a flexible solar cell on top is shown in Figure 3.11 [84]. The positive terminal of the solar cell is connected to the monopole conductor, while the negative terminal of the solar cell is connected to the ground conductor of the monopole through a conductive line near the top of the monopole, which has been shown in simulation to have a minimum effect in distorting the input impedance and the radiation pattern of the monopole antenna. The input s-parameters of the antenna with and without the solar cell are shown in Figure 3.11b, where we can see that the solar cell affects very little the input impedance of the antenna. Furthermore, measured radiation patterns of the solar antenna are shown in Figure 3.12 [85]. One can see that the presence of the solar cell has little effect on the antenna maximum gain and copolarization radiation pattern, and it results in an increase in the cross-polarization radiation pattern.

An example of a slot antenna integrating cells on top of the conducting areas surrounding the slot is shown in Figure 3.13 [84]. The antenna is a cavity backed slot antenna, where the cavity is formed by metalized vias in the substrate implementing an antenna in substrate integrated circuit technology.

An example of a textile solar antenna is shown in Figure 3.14 [83]. A quarter wavelength shorted patch antenna is used as the basis of the solar antenna, and the solar cell wiring is taken from the shorted side of the patch, thus having a minimum effect on the antenna performance.

Table 3.2 includes selected recent solar antenna designs in the literature and summarizes their properties.

Finally, one interesting application is that of integrating solar cells with RFID tag antennas in order to provide an additional source of power to the tag other than the RF power and consequently increase their operating range. The idea

https://doi.org/10.1017/9781139600255.004 Published online by Cambridge University Press

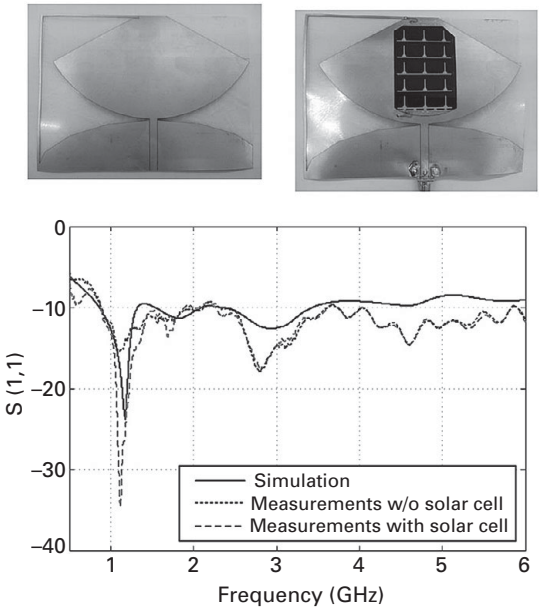

Figure 3.11 Flexible solar cell integrated on top of an ultrawideband monopole on a PET substrate demonstrated in [84]: photo of the antenna with and without the solar cell and input s-parameters. ©2014 IEEE. Reprinted, with permission from [84]

Table 3.2 Selected solar antenna publications.

Reference	Antenna type	Frequency
[77]	Patch antenna, linear polarization	2.25 GHz
[79]	Slot antenna, Ultralam substrate	3.87 GHz
[80]	UWB monopole antenna, FR4 substrate	3.1 GHz–10.6 GHz
[83]	Shorted patch antenna, textile substrate	915 MHz
[82]	UWB monopole, PET substrate	0.85 GHz–6 GHz
[81]	Patch antenna, transparent conductor AgHT-4	3.4 GHz–3.8 GHz
[86]	Slot antenna array underneath solar cell	2.4 GHz

was initially proposed in [87], where a printed monopole antenna with a solar cell on top of the monopole ground and an RFID tag was envisioned. The challenge is how to supply the RFID tag IC with the dc power from the solar cell. While there exist tags with an external input port separate from the RF port that accepts dc power, tag ICs typically only have two RF input ports. In [88], solar cells were integrated on RFID tag dipole arms (Figure 3.15) and the dc signal from the solar cells was converted to an RF signal by powering an RF oscillator placed next to the tag IC. The RF signal from the oscillator was fed to the input RF ports of the tag IC, therefore enabling the topology to be compatible with common type RFID tag ICs. The solar RFID tag is shown in Figure 3.15.

https://doi.org/10.1017/9781139600255.004 Published online by Cambridge University Press

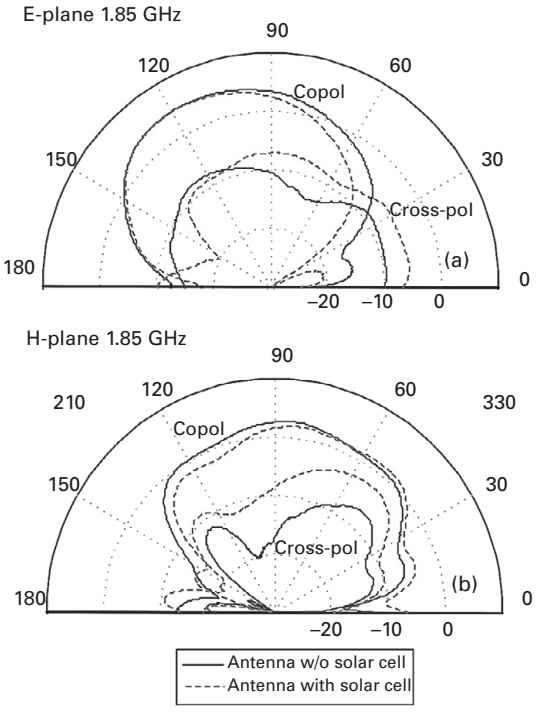

Figure 3.12 Measured (a) E-plane and (b) H-plane radiation patterns of the solar monopole antenna shown in Figure 3.11a at 1.85 GHz [85].

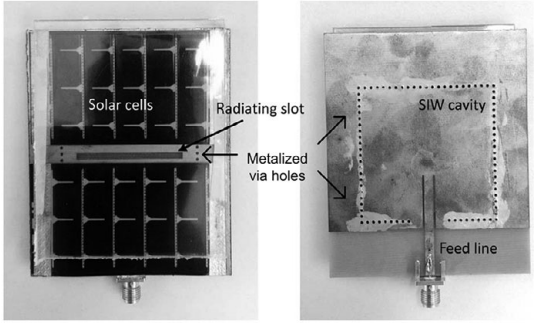

Figure 3.13 Cavity-backed substrate-integrated waveguide slot antenna with solar cells. ©2014 IEEE. Reprinted, with permission from [84]

3.11 Problems and Questions

1. What is the physical phenomenon that the operation of solar cells is based on, when was it discovered, and by who?
2. What is the measure 1 sun?
3. What is the AM1.5G standard?

https://doi.org/10.1017/9781139600255.004 Published online by Cambridge University Press

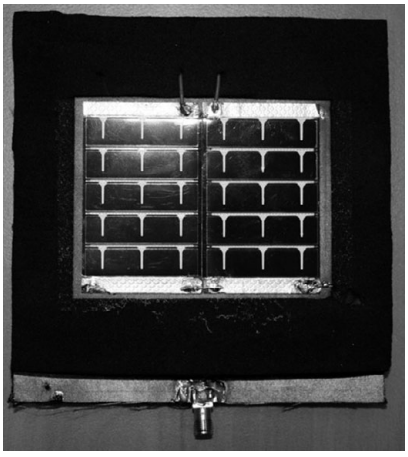

Figure 3.14 Solar patch antenna on textile substrate courtesy of Prof. Hendrik Rogier, Ghent University [83].

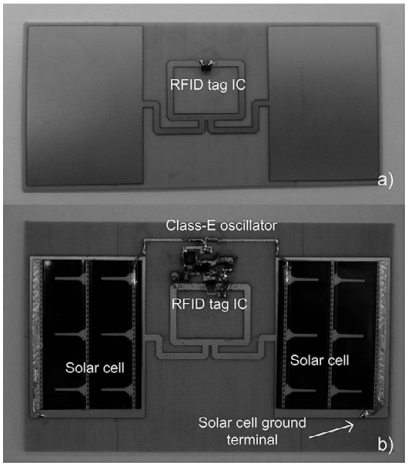

Figure 3.15 Solar power harvesting assisted RFID tag: a) original tag and b) modified tag with solar cells and oscillator circuit. ©2012 IEEE. Reprinted, with permission from [88]

4. What is the ultimate solar cell efficiency?
5. What is the detailed balance limit?
6. Compute the maximum value of ultimate solar cell efficiency and the corresponding band-gap value corresponding to the AM0 and AM1.5G spectra.
7. Name four characterizing parameters of solar cells. What is the fill factor of a solar cell?
8. What is the maximum solar cell efficiency based on the detailed balance limit for a silicon solar cell ($E_g = 1.1$ eV) and for a GaAs solar cell ($E_g = 1.424$ eV),

https://doi.org/10.1017/9781139600255.004 Published online by Cambridge University Press

assuming $T_s = 6{,}000$ K, $T_c = 300$, $f_w = 2.18 \cdot 10^{-5}$, and no radiative recombination.

9. Compute the ultimate efficiency contours of tandem solar cells with three band gaps. What are the optimum band-gap energies and what is the maximum theoretical efficiency?

https://doi.org/10.1017/9781139600255.004 Published online by Cambridge University Press